Cross-sectional mapping for refined beam elements with applications to shell-like structures

(Article begins on next page)

17 April 2024

Cross-sectional mapping for refined beam elements with applications to shell-like structures

A. Pagani[*], A.G. de Miguel[†], E. Carrera[‡]

Department of Mechanical and Aerospace Engineering, Politecnico di Torino, Corso Duca degli Abruzzi 24, 10129 Torino, Italy.

Abstract

This paper discusses the use of higher-order mapping functions for enhancing the physical representation of refined beam theories. Based on the Carrera Unified Formulation (CUF), advanced one-dimensional models are formulated by expressing the displacement field as a generic expansion of the generalized unknowns. According to CUF, a novel physically/geometrically consistent model is devised by employing Legendre-like polynomial sets to approximate the generalized unknowns at the cross-sectional level, whereas a local mapping technique based on the blending functions method is used to describe the exact physical boundaries of the cross-section domain. Classical and innovative finite element methods, including hierarchical p-elements and locking-free integration schemes, are utilized to solve the governing equations of the unified beam theory. Several numerical applications accounting for small displacements/rotations and strains are discussed, including beam structures with cross-sectional curved edges, cylindrical shells, and thin-walled aeronautical wing structures with reinforcements. The results from the proposed methodology are widely assessed by comparisons with solutions from the literature and commercial finite element software tools. The attention is focussed on the high computational efficiency and the marked capabilities of the present beam model, which can deal with a broad spectrum of structural problems with unveiled accuracy in terms of geometrical representation of the domain boundaries.

Keywords: Refined beam theories, Finite element method, Carrera unified formulation, Hierarchical Legendre expansions, Mapping, Blending functions.

---

[*]Assistant Professor, e-mail: alfonso.pagani@polito.it
[†]Marie Curie PhD Student, e-mail: alberto.garcia@polito.it
[‡]Professor of Aerospace Structures and Aeroelasticity, e-mail: erasmo.carrera@polito.it

1 Introduction

This paper presents a novel refined beam model with shell-like capabilities that makes use of a higher-order mapping methodology to enhance the geometrical accuracy for the modelling of physical boundaries of curved cross-sections domains. Beam theories have become an important tool for the study of a large number of structural problems, but still their usage is limited by the simplicity of the geometries they can deal with. The main idea is to develop beam models able of representing the exact geometry of the beam cross-section regardless of the complexity of the shape and the refinement of the theory kinematics.

One-dimensional theories are commonly used for many applications in several engineering fields such as aerospace, civil or bio-mechanical fields, in which slender structures are frequent. Commonly, beam theories make use of a reduced number of degrees of freedom and they have demonstrated to be very efficient in many cases in comparison with more cumbersome 2D and 3D models. Although classical beam theories, introduced by Euler [1] and Timoshenko [2], are only suitable for a limited class of problems, in particular long homogeneous beams subjected to bending, the development of more sophisticated models with enriched kinematics enables to accurately solve problems that usually require the use of 2D or 3D elements, with a great advantage in terms of computational costs. Many refined beam theories are available in the literature. A discussion of various of these models can be found, for instance, in Kapania and Raciti [3, 4] and in Carrera et al. [5]. The exact solution of the Timoshenko beam theory was used by Reddy [6] to develop a locking-free finite element model. Higher-order beam theories were also discussed by Vinayak et al. [7], who made use of the Lo-Christensen-Wo theory to develop finite element formulations, with a particular attention on flexure of beams and plates. An approximation of shear stresses in prismatic beams was introduced by Gruttmann et al. [8], who considered the Saint-Venànt torsion and bending. The application of this model to thin-walled beams was then presented in Gruttmann and Wagner [9]. The effects of higher-order shear deformation theories were studied by Petrolito [10], with a comparison against classical beam theories. The Generalized Beam Theory (GBT), introduced by Schardt [11] and developed by Davids et al. [12, 13], represented an extension of the conventional engineering beam theories by considering the cross-section distortion. The GBT was employed by Silvestre and Camotim [14, 15] for the study of thin-walled orthotropic beams and then by Silvestre [16] to analyse the elastic buckling behaviour of circular hollow sections, such as cylinders and tubes. On non-linear beam kinematics, Simo and Vu-Quoc [17] presented an extension of the finite strain beam formulation to incorporate shear and torsion-warping phenomena and Pimenta and Campello [18] introduced a fully non-linear rod model that accounted for in-plane cross-sectional changes and out-of-plane warping. Other contributions including cross-sectional in-plane distorsion and warping for thin-walled beams can be found in Gonçalves et al. [19] and Campello and Lago [20], among the others.

In this framework, the Carrera Unified Formulation (CUF), developed by Carrera and his colleagues during the past two decades, was devised to overcome the limitations of conventional beam models by describing the kinematics of structural theories in a unified manner

that allows to write the finite element arrays and, thus, the governing equations in a hierarchical and compact form. Initially, Carrera [21, 22] introduced CUF for two-dimensional structural and multi-field problems. The extension of CUF to beam models was proposed by Carrera and Giunta [23], where the authors developed N-order approximations based on MacLaurin polynomial expansions of the primary mechanical variables. Taking advantage of the generality of the CUF, any theory of structure can be implemented in a straightforward way. A detailed description of the most relevant theories based on CUF is further included in this paper.

The quality of the geometric approximation represents a major issue not only for beam models such as the aforementioned ones, but in general for the mathematical description of structural problems, specially in the domain of the Finite Element Method (FEM). The finite element space is characterised by three main factors, i.e. the finite element mesh, the polynomial order of the elements and the mapping functions. A good approximation of a certain structural problem requires a proper combination of these parameters to minimize the error inherently introduced. In conventional finite element methods, also known to as the h-version of FEM, the solution accuracy and, eventually, the approximation of the geometrical domain are mutually enhanced by reducing the size of the isoparametric elements. This technique implies that complex geometrical representations may induce the use of highly refined meshes. On the other hand, in the p-version of FEM, introduced by Szabó and Babŭska [24], the mesh is fixed and the quality of the approximation is determined by the polynomial degree of the elements. The coarse discretizations used for the p-version make necessary to have a good geometric representation of the physical domain to keep the mapping errors negligible. Gordon and Hall [25] presented a method to introduce the exact geometrical description of the boundaries into the mapping functions, called the blending function method. This method, which is described with more detail hereafter, has demonstrated to be very convenient to define curved domains of p-version finite elements, as shown in Düster et al. [26]. A generalization of the isoparametric mapping to p-version elements was introduced by Királyfalvi and Szabó [27], who developed a technique denoted to as quasi-regional mapping, that makes use of piecewise polynomials to represent the curved boundaries and the blending function method to define the mapping functions. Another way to deal accurately with complex domain descriptions was inspired by Computer Aided Design (CAD) tools to Hughes et al. [28], who formulated the so-called isogeometric analysis. The isogeometric analysis makes use of FEM basis functions constructed from non-uniform rational b-splines (NURBS) and represents a tentative to link mesh generation and CAD geometry. Nevertheless, it is important to underline that, unlike the p-version of FEM, the isogeometric analysis is, in fact, an isoparametric formulation.

Although these technologies for the geometrical description of the problem boundaries have been introduced and widely utilized in FEM to represent the reference domain (e.g., the beam axis in 1D models and the plate mid-plane in the case of 2D models), blending functions as well as NURBS can be opportunely employed to develop refined kinematics

theories of structures. In this work, for example, blending functions are used along with a refined beam structural model to represent the cross-section domain correctly so as to allow for the exact evaluation of the classical and higher-order cross-sectional moment parameters. It should be underlined that the present methodology is restricted to the small displacements and strains regime, without any loss of generality.

The paper is structured as follows: first, an overview of different variable kinematic CUF models is presented in Section 2, with a focus on Hierarchical Legendre Expansions. Particular attention is given to the application of these models to curved and complex cross-sections through mapping techniques. The basis of the finite element method for beams in the framework of CUF is provided in Section 3, including a description of the fundamental nucleus of the stiffness matrix derived from the Principle of Virtual Displacements (PVD). The numerical results, obtained for several examples of beam and shell-like structures, are addressed in Section 4, and the main conclusions of the work are outlined in Section 5.

2   Refined CUF models

According to Washizu [29], the displacement field of beam theories can be enriched with an arbitrary number of higher-order terms in order to overcome the limitations of classical models and to deal with complex mechanics and phenomena, such as torsion, warping, and in-plane deformations. In the framework of CUF, the displacement field is expressed in a unified manner as a generic expansion of the generalized unknowns by arbitrary functions of the cross-section domain coordinates:

$$\mathbf{u}(x,y,z) = F_\tau(x,z)\mathbf{u}_\tau(y) \quad \tau = 1,2,...,M, \tag{1}$$

where $\boldsymbol{u}_\tau(y)$ is the vector of general displacements laying along the beam axis y. According to Einstein notation, τ denotes summation. $F_\tau(x,z)$ corresponds to the expanding functions on the cross-section, Ω, which is defined in the Cartesian plane $x-z$, and M is the number of terms in the expansion. In fact, the choice of $F_\tau(x,z)$ determines the class of beam theory to be adopted. A brief introduction of the main CUF beam theories that have been introduced in the past few years is provided in the following, with a focus on HLE.

2.1   Taylor Expansions

Taylor Expansion (TE) models employ hierarchical sets of 2D polynomials from MacLaurin series of the type $x^i z^j$ for the definition of $F_\tau(x,z)$. For instance, the second order model, N=2, makes use of constant, linear and quadratic expansion terms:

$$
\begin{aligned}
u_x(x,y,z) &= u_{x_1}(y) + x\, u_{x_2}(y) + z\, u_{x_3}(y) + x^2\, u_{x_4}(y) + xz\, u_{x_5}(y) + z^2\, u_{x_6}(y) \\
u_y(x,y,z) &= u_{y_1}(y) + x\, u_{y_2}(y) + z\, u_{y_3}(y) + x^2\, u_{y_4}(y) + xz\, u_{y_5}(y) + z^2\, u_{y_6}(y) \\
u_z(x,y,z) &= u_{z_1}(y) + x\, u_{z_2}(y) + z\, u_{z_3}(y) + x^2\, u_{z_4}(y) + xz\, u_{z_5}(y) + z^2\, u_{z_6}(y).
\end{aligned}
\tag{2}
$$

It is clear that the classical beam theories can be defined as particular cases of TE of first order (N=1), including the constant and linear terms in Eq. (2). In these class of models, the generalized displacement variables (i.e. displacements and their derivatives) are expanded globally over the cross-section from the beam axis. The polynomial order of the theory is then increased in a straightforward manner by adding higher-order terms to the kinematic field, enhancing the accuracy of the approximation. TE models have been extensively studied in many works, see for example [30, 31, 32, 33, 34].

2.2 Lagrange Expansions

Lagrange Expansion (LE) beam theories are based on the use Lagrange-type polynomials as generic expansions on the beam section domain, F_τ. The cross-section physical surface is discretize into a number of local expansion sub-domains, whose polynomial degree depends on the type of Lagrange expansion employed. Three-node linear L3, four-node bilinear L4, nine-node quadratic L9, and sixteen-node cubic L16 polynomials have been developed in the framework of CUF. For the sake of brevity, their expressions are not included here, but they can be found in Carrera and Petrolo [35]. For instance, the kinematic field of the L9 beam model reads:

$$
\begin{aligned}
u_x(x,y,z) &= F_1(x,z)\, u_{x_1}(y) + F_2(x,z)\, u_{x_2}(y) + F_3(x,z)\, u_{x_3}(y) + ... + F_9(x,z)\, u_{x_9}(y) \\
u_y(x,y,z) &= F_1(x,z)\, u_{y_1}(y) + F_2(x,z)\, u_{y_2}(y) + F_3(x,z)\, u_{y_3}(y) + ... + F_9(x,z)\, u_{y_9}(y) \quad (3) \\
u_z(x,y,z) &= F_1(x,z)\, u_{z_1}(y) + F_2(x,z)\, u_{z_2}(y) + F_3(x,z)\, u_{z_3}(y) + ... + F_9(x,z)\, u_{z_9}(y),
\end{aligned}
$$

where F_1,...,F_9 form a usual quadratic Lagrange polynomial set. The main feature of LE models is that they make use of local expansions of pure displacement variables, being these arbitrary placed over the cross-section surface. This characteristic enables to capture complex 3D-like solutions at a global-local scale and to increase the accuracy of the solution in particular zones of interest. Recently, LE beam models have been employed for the Component-Wise (CW) analysis of composite laminates at various scales [36], aerospace structures [37, 38], civil constructions [39, 40], and marine ship hulls [41].

2.3 Hierarchical Legendre Expansions

This class of CUF beam theories was devised in Carrera et al. [42] by adopting hierarchical series of Legendre-type polynomials to expand the generalized displacement variables over the cross-section. Hierarchical Legendre Expansion (HLE) models combine the main features of the previous CUF beam models, i.e. the hierarchy of the high-order terms of TE and the geometric discretization of the beam section surface of LE. HLE models employ a set of hierarchical Legendre-like polynomials (see [24, 43]) as F_τ generic functions on the cross-section domains. These functions are utilized in this work in conjunction with a high-order mapping technique to generate non-isoparametric expansions over the cross-section that allow to capture the exact geometry of curved surfaces, as described in the next section. Figure 1 shows
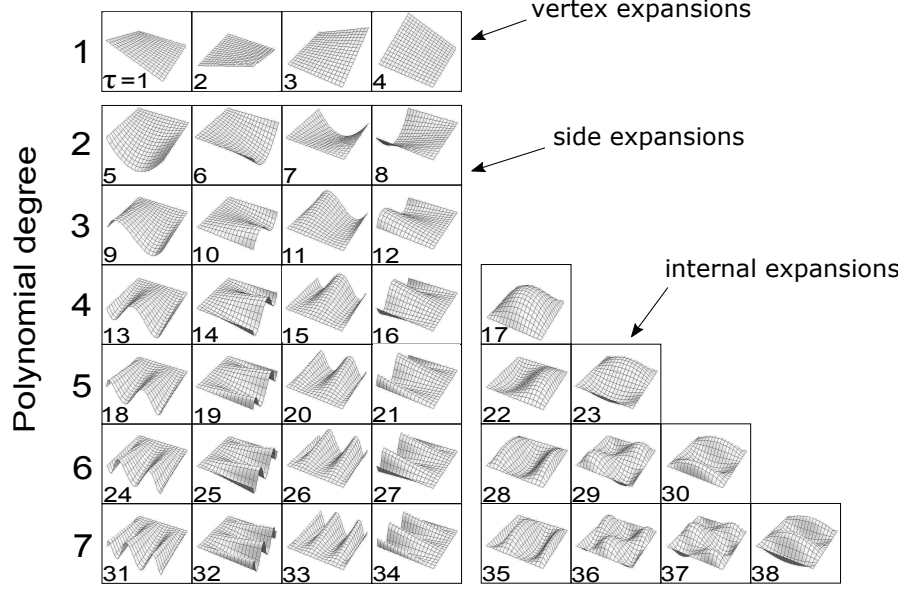
Figure 1: Linear to seventh-order, hierarchical Legendre-type F_τ expansion used for HLE models.

all the polynomials used in HLE beam theories from the 1st to the 7th order. Quadrilateral nodal, edge and internal expansions conform the hierarchical set, see [44].

Vertex expansions The nodal or vertex modes are analogue to the linear Lagrange polynomials (L4). They are defined as follows:

$$F_\tau = \frac{1}{4}(1 - r_\tau r)(1 - s_\tau s) \qquad \tau = 1, 2, 3, 4, \tag{4}$$

where r and s vary over the domain between -1 and $+1$, and r_τ and s_τ represent the vertex coordinates in the natural system of coordinates.

Side expansions The side modes are defined for $p \geq 2$, being p the polynomial order, and their expressions are:

$$F_\tau(r, s) = \frac{1}{2}(1 - s)\phi_p(r) \qquad \tau = 5, 9, 13, 18, ... \tag{5}$$

$$F_\tau(r, s) = \frac{1}{2}(1 + r)\phi_p(s) \qquad \tau = 6, 10, 14, 19, ... \tag{6}$$

$$F_\tau(r, s) = \frac{1}{2}(1 + s)\phi_p(r) \qquad \tau = 7, 11, 15, 20, ... \tag{7}$$

$$F_\tau(r, s) = \frac{1}{2}(1 - r)\phi_p(s) \qquad \tau = 8, 14, 16, 21, ..., \tag{8}$$

where ϕ_p corresponds to the one-dimensional internal Legendre-type modes, see [24, 42] and Eq. (31). These functions are defined in such a way that the C^0 continuity at the interface of cross-section domains is assured.

Internal expansions The F_τ internal expansions are included for $p \geq 4$ and they vanish at all the edges of the quadrilateral domain. In total, there are $(p-2)(p-3)/2$ internal polynomials. For instance, the sixth-order polynomial set contains three internal expansions (see Fig. 1), which are

$$F_{28}(r,s) = \phi_4(r)\phi_2(s) \tag{9}$$

$$F_{29}(r,s) = \phi_3(r)\phi_3(s) \tag{10}$$

$$F_{30}(r,s) = \phi_2(r)\phi_4(s). \tag{11}$$

It is important to remark that the hierarchy of this model implies that the set of functions of a particular order contains all the polynomials of the lower degrees. As far as the sixth-order HLE model is concerned, the set of functions of the kinematic expansion terms includes the internal polynomials introduced in Eqs. (9), (10) and (11), plus all the internal, side and vertex functions of the same polynomial order and below, i.e $\tau = 1, ..., 30$. As a consequence, the accuracy of the approximation can be enhanced by increasing the polynomial order of the theory, which leads to the use of coarse discretizations at the cross-sectional level and the need of a proper mapping for large expansion domains.

2.4 Cross-section mapping

Once the kinematics of the beam are defined, the calculation of the stiffness terms goes through the evaluation of cross-sectional moment parameters (e.g., first and second moments of area in classical beam theories). These generalized moment of area are computed by integrating the cross-sectional functions F_τ over the cross-section of the beam, Ω. Hence, it is clear that the correct geometrical description of Ω is of fundamental importance when dealing with complex geometries and curved-section beams.

The present paper takes inspiration from FEM to respond to the aforementioned demand. As it is known, conventional finite elements make use of isoparametric formulations to map the geometry of a structural problem. This means that the shape of the physical boundaries of the domain is described by the same functions that are used to interpolate the unknown variables. In the CUF framework, this approach is also employed for the mapping of the cross-section in LE models. However, as for the p-version of FEM, the elevated expansion orders of the HLE enable the use of coarse domain discretizations of the cross-section surface. It is in this context that it becomes important to represent the curved boundaries of large domains accurately through an independent description of the geometry. The blending function method, introduced by Gordon and Hall [25], serves to this purpose.

First, let us consider the mapping functions of a certain expansion domain, see for example Fig. 2. These mapping functions, represented by $\mathbf{Q}$, are defined in the x-z plane of the cross-
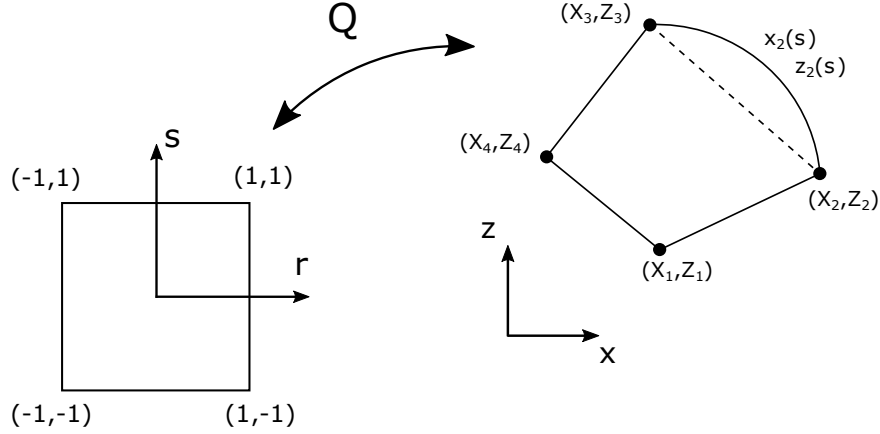
Figure 2: Mapping of a cross-sectional quadrilateral domain with one curved edge, see [24]. The mapping functions are represented by $\mathbf{Q} = (Q_x \ Q_z)$.

section surface as:

$$x = Q_x(r, s) \tag{12}$$

$$z = Q_z(r, s), \tag{13}$$

where r and s are the coordinates in the natural plane of the quadrilateral domain.

First-order mapping

If isoparametric first-order expansion domains are used, as for example in Lagrange-type L4 CUF models, the approximation of the geometry is obtained through linear mapping. The mapping functions of quadrilateral elements are described as follows

$$
\begin{aligned}
x = Q_x(r, s) = \quad & \tfrac{1}{4}(1 - r)(1 - s)X_1 + \tfrac{1}{4}(1 + r)(1 - s)X_2 \\
& + \tfrac{1}{4}(1 + r)(1 + s)X_3 + \tfrac{1}{4}(1 - r)(1 + s)X_4
\end{aligned}
\tag{14}
$$

$$
\begin{aligned}
z = Q_z(r, s) = \quad & \tfrac{1}{4}(1 - r)(1 - s)Z_1 + \tfrac{1}{4}(1 + r)(1 - s)Z_2 \\
& + \tfrac{1}{4}(1 + r)(1 + s)Z_3 + \tfrac{1}{4}(1 - r)(1 + s)Z_4,
\end{aligned}
\tag{15}
$$

which in a simplified manner can be rewritten as:

$$\mathbf{x} = F_\tau(r, s) \, \mathbf{X}_\tau \quad i = 1, ..., 4, \tag{16}$$

where $\mathbf{x} = (x \ z)^T$ is the geometry vector of the cross-section, $\mathbf{X}_\tau = (X_\tau \ Z_\tau)^T$ are the vertex of the quadrilateral domain and τ denotes summation. F_τ are exactly the same linear functions as used in the description of the kinematics of the L4 beam model. The lector can notice that this expression is, in fact, analogous to the Eq. (1) used to define the displacement field and it does not allow to represent curved cross-section edges, like the one in Fig. 2.

8

Second-order mapping

Extending this procedure to biquadratic quadrilateral domains, it is possible to represent curved boundaries by second-order polynomials. This is the case of Lagrange-type L9 beam models, whose cross-sectional mapping, in the same compact notation, can be expressed as

$$\mathbf{x} = F_\tau(r, s)\,\mathbf{X}_\tau \quad i = 1, ..., 9, \tag{17}$$

where $F_\tau(r, s)$ correspond to the biquadratic expansions polynomials of the L9 model. Again, the geometry of the domain is represented by the same interpolation functions of the kinematic field, like in Eq. (1). Therefore, this approach is also considered as isoparametric mapping, and it allows to generate slightly curved domains.

The blending function method

As it has been mentioned previously, when using HLE it is of key importance to ensure that the representation of the domain is accurate enough to make the geometric approximation error negligible. The blending function method enables one to include the exact shape of the cross-section by introducing parametric polynomials of an arbitrary order to describe the shape of curved edges. The boundary surfaces of the domains are incorporated directly into the mapping functions and no geometrical error is introduced in the modelling procedure. Obviously, this approach cannot be considered as isoparametric since the mapping functions do not correspond with the expansion functions, F_τ.

To present the method, first we consider a quadrilateral domain in which one of the sides is curved, see Fig. 2. In that domain, the coordinates of the curved edge are represented by the parametric functions $x = x_2(s)$ and $z = z_2(s)$. If a cubic parametrization is chosen, the functions take the form of third-order polynomials as

$$x_2(s) = a_x + b_x s + c_x s^2 + d_x s^3 \tag{18}$$

$$z_2(s) = a_z + b_z s + c_z s^2 + d_z s^3. \tag{19}$$

These functions are defined in such a way that $x_2(-1) = X_2$, $x_2(1) = X_3$, $z_2(-1) = Z_2$ and $z_2(1) = Z_3$, with $-1 < (r, s) < 1$. Then, according to the blending function method, the mapping functions are written as:

$$x = Q_x(r, s) = F_\tau(r, s)X_\tau + \left(x_2(s) - \left(\frac{1-s}{2}X_2 + \frac{1+s}{2}X_3 \right) \right)\frac{1+r}{2} \tag{20}$$

$$z = Q_z(r, s) = F_\tau(r, s)Z_\tau + \left(z_2(s) - \left(\frac{1-s}{2}Z_2 + \frac{1+s}{2}Z_3 \right) \right)\frac{1+r}{2}, \tag{21}$$

where $\tau = 1, ..., 4$. In this expression, the first term corresponds to the linear mapping functions defined in Eq.(14) and (15). The second addend, instead, accounts for the difference between the parametric functions, $x_2(s)$ and $z_2(s)$, and the x and z coordinates of the straight line that connects vertices 2 and 3 of the quadrilateral domain. The term $\frac{1+r}{2}$ is the linear
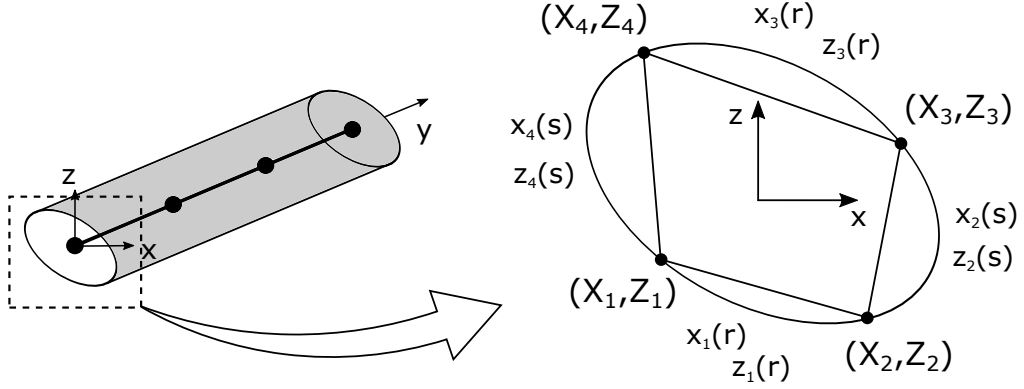
Figure 3: Mapping of the cross-section domain by the blending function method.

blending function and it takes the unity value along side 2 and it goes to zero on side 4, ensuring that the mapping of one side does not have any effect on the opposite one.

In the general case of a quadrilateral domain with all sides curved, the previous procedure is expanded to all the edges to have

$$x = Q_x(r,s) = \frac{1}{2}(1-s)x_1(r) + \frac{1}{2}(1+r)x_2(s) + \frac{1}{2}(1+s)x_3(r) \tag{22}$$

$$+\frac{1}{2}(1-r)x_4(s) - F_\tau(r,s)X_\tau \tag{23}$$

$$z = Q_z(r,s) = \frac{1}{2}(1-s)z_1(r) + \frac{1}{2}(1+r)z_2(s) + \frac{1}{2}(1+s)z_3(r) \tag{24}$$

$$+\frac{1}{2}(1-r)z_4(s) - F_\tau(r,s)Z_\tau, \tag{25}$$

where all the sides of the element have been represented by parametric functions. Figure 3 shows the application of the blending function method in the framework of HLE beam models. This method allow us to reproduce the exact shape of complex section geometries with the use of a minimum number of local expansions. The main advantages of the use of HLE mapped models are two: first, the reduction of the error related to the geometrical approximation, and second, but not less important, the substantial savings in terms of computational cost and modelling time. Once the cross-section discretization is fixed, the polynomial order of the expansion domains can be easily trimmed to a desired level of accuracy, which leads to a efficient computation of the solutions.

3 Finite element formulation

The main advantage of CUF is that it allows to write the governing equations and the FEM arrays in a unified and hierarchal manner which is affected neither by the choice of the theory of structure, represented by F_τ, nor by the FE shape functions N_i. In fact, the class (e.g., TE, LE, HLE) and the order of the beam theory becomes in this way an input of the model. The generalized displacements are described as a function of the unknown nodal vector, $\mathbf{q}_{\tau i}$,

and the 1D shape functions, N_i, as follows

$$\mathbf{u}_\tau(y) = N_i(y)\mathbf{q}_{\tau i}, \qquad i = 1, 2, ..., n, \tag{26}$$

where n is the number of shape functions per element, and the unknown nodal vector is defined as

$$\mathbf{q}_{\tau i} = \left\{ \begin{array}{ccc} q_{x\tau i} & q_{y\tau i} & q_{z\tau i} \end{array} \right\}^T. \tag{27}$$

The beam element formulation depends on the choice of the shape functions $N_i(y)$. Two different beam elements are employed in the present work: Lagrange-type and Legendre-type elements.

Lagrange beam elements. Lagrange-type polynomials are the most common choice in finite element formulations. They are used to interpolate the unknown displacement variables at the element nodes, whose number determines the polynomial order of the shape functions N_i. For the sake of brevity, their expressions are not included here, but they can be found in Carrera et al. [30] for linear, quadratic and cubic interpolations.

Legendre beam elements. The interpolation of the unknowns is conducted by employing a hierarchical set of 1D Legendre-type polynomials, $L_{\hat{i}}$, which leads to a set of shape functions of the following form

$$N_1(r) = \frac{1}{2}(1 - r) \tag{28}$$

$$N_2(r) = \frac{1}{2}(1 + r) \tag{29}$$

$$N_i(r) = \phi_{i-1}(r), \qquad i = 3, 4, ..., n, \tag{30}$$

where r correspond to the local coordinate in the natural domain of the beam element [-1,1], and $\phi_j(r)$ is

$$\phi_{\hat{i}}(r) = \sqrt{\frac{2\hat{i} - 1}{\hat{i}}} \int_{-1}^{r} L_{\hat{i}-1}(x) \, dx, \quad \hat{i} = 2, 3, 4, ..., \tag{31}$$

as defined in [24, 42]. The set of polynomials is defined in a hierarchical manner and, as a consequence, the polynomial order of the element can be increased straightforwardly by adding internal shape functions of higher orders. The approximation error is, in fact, reduced by following a p-refinement method in which the longitudinal mesh is fixed and the order is trimmed to a desired level of accuracy.

3.1   Fundamental nuclei

The principle of virtual displacements (PVD) is recalled hereinafter to obtain the governing equations. Basically, the PVD states that the virtual variation of the internal work must be

equal to the virtual variation of the external work for the structure to be in equilibrium,

$$\delta L_{\text{int}} = \delta L_{\text{ext}}. \tag{32}$$

In addition, the internal work corresponds to the elastic strain energy

$$\delta L_{int} = \int_l \int_\Omega \delta \boldsymbol{\varepsilon}^T \boldsymbol{\sigma} \, d\Omega \, dy, \tag{33}$$

where l is the length of the beam and Ω represents the surface of cross-section domain. By considering the CUF kinematic field included in Eq. (1), the finite element discretization of Eq. (26) and the 3D constitutive and geometrical relations[1], the expression of the internal work can be rewritten in a compact manner as follows (see [45])

$$\delta L_{\text{int}} = \delta \mathbf{q}_{\tau i}^T \mathbf{K}^{\tau s i j} \mathbf{q}_{sj}, \tag{34}$$

where $\boldsymbol{K}^{\tau s i j}$ represents the 3×3 fundamental nucleus of the element stiffness matrix. In the present work, $\boldsymbol{K}^{\tau s i j}$ is derived under the assumptions of small displacements and strains. An important fact to remark is that the formal expression of the fundamental nucleus is invariant with the choice of both the theory of structure, F_τ, and the beam shape functions, N_i. For the sake of completeness, its components for isotropic structures are expressed in the following:

$$
\begin{aligned}
K_{\alpha\alpha}^{\tau s i j} &= (\lambda + 2G) \int_l N_i \, N_j \, dy \int_\Omega F_{\tau,x} F_{s,x} \, d\Omega \; + \; G \int_l N_i \, N_j \, dy \int_\Omega F_{\tau,z} F_{s,z} \, d\Omega + \\
&\quad + G \int_l N_{i,y} \, N_{j,y} \, dy \int_\Omega F_\tau F_s \, d\Omega \\
K_{\alpha\beta}^{\tau s i j} &= \lambda \int_l N_i \, N_{j,y} \, dy \int_\Omega F_\tau F_{s,x} \, d\Omega + G \int_l N_{i,y} \, N_j \, dy \int_\Omega F_{\tau,x} F_s \, d\Omega,
\end{aligned}
\tag{35}
$$

where $\alpha, \beta = x, y, z$. It is intended, in fact, that all the nine components of the stiffness nucleus can be obtained by permutations from Eq. (35). It should be underlined that the components of the fundamental nucleus in Eq. (35) depend only on the material coefficients, λ and G, the integrals of the shape functions along the longitudinal axis and the integrals of the expansion functions above the cross-section domain, being the last two independent from each other. All the integrals over l and Ω are computed numerically using a Gauss-Legendre scheme. If not differently specified, a selective reduced integration scheme is adopted for the calculation of the integrals of the shape functions N_i to attenuate the shear locking effects. Any refined beam model can be automatically formulated by expanding the fundamental nucleus within the stiffness matrix on τ, s, i, and j. More details about CUF and the expansion of the fundamental nuclei can be found in Carrera at al. [45].

---

[1]Note that, as in the case of this paper, the use of 3D constitutive relations does not entail Poisson locking if higher-order kinematics are employed on the cross-section, see [35, 45].
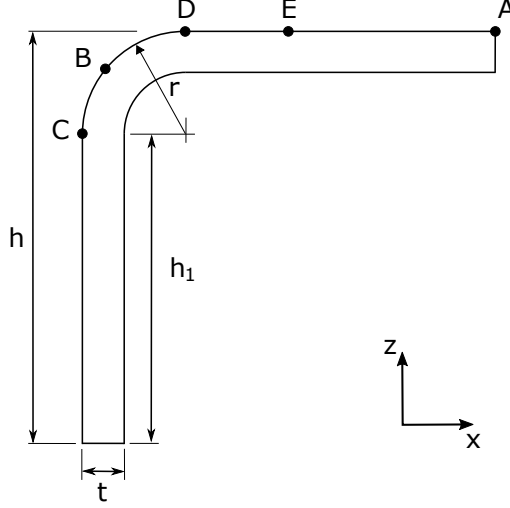
Figure 4: L-shaped beam geometry.

4 Numerical results

A number of static analyses are included in this section to assess the validity of the mapping techniques on HLE models. The numerical results are compared against those from beam, shell and solid models generated with the commercial software MSC Nastran and, when possible, those found in the literature. The examples have been selected to show the capabilities of the present formulation to deal with a wide range of structural problems, including thin-walled beams, shell-like components, and aerospace structures.

4.1 L-angle beam

An L-section beam is used first to assess the accuracy of the HLE beam theory applied to curved cross-section geometries. This type of components are extensively used as stiffeners in many applications, such as wing boxes or civil structures. The section geometry can be found in Fig. 4, being its characteristics the following: the total height, h, is equal to 20 mm; both vertical and horizontal flanges are as long as $h_1 = 15$ mm; the thickness, t, is equal to 2 mm; the radius of curvature is $r = 5$ mm. The total length of the beam is 1 m, which means a slenderness ratio, L/h, of 50. The characteristics of the material are the ones of a typical aluminum alloy for aerospace applications with Young modulus, E, equal to 75 GPa, and Poisson ratio, $\nu = 0.33$. A clamped-free configuration was selected for the assessment and a point force of $F = -50$ N of magnitude in the z-direction was applied at the tip section in correspondence of point E (see Fig. 4).

Table 1 reports the results in terms of displacements and stresses of the L-angle beam. Displacements on the three directions are calculated at the upper corner of the top flange at the tip section (Point A in Fig. 4), whereas longitudinal, σ_{yy} and shear stresses, σ_{yz} and σ_{xy}, are measured at different points of the cross-section (Points B, C and D in in Fig. 4) at $y = 0.2$ m. Classical analytical solutions of this structural problem have been obtained

accounting for bending, shear, torsion and secondary warping. The displacements shown in the first row of Table 1 have been calculated using the Euler-Bernoulli beam theory [1] accounting for the bending effects. The contribution of the deflection due to shear pappears in the second row and the contribution of torsion is included in the third row. The theory of the warping torsion of Vlasov [46] has been recalled in the present assessment to include the restrained warping. According to it, the torsional angle, θ, is described along the beam axis by the following differential equation:

$$EJ_\omega \frac{d^4\theta}{dy^4} - GJ_t \frac{d^2\theta}{dy^2} = m_y, \tag{36}$$

where EJ_ω is the warping stiffness, GJ_t is the torsion stiffness and m_y is the distributed torsion moment along the beam. One may notice that the influence of the shear deflection on the displacement solutions is relatively small due to the moderately high slenderness ratio of the beam under study. The contribution of the secondary warping to the longitudinal displacement, u_y, and the stress solutions is negligible in this case due to the cross-sectional geometry of the L-angle beam considered and therefore it has not been included in Table 1. The longitudinal and shear stresses have been computed utilizing the well-known Navier and Grashof's formulas for bending, respectively. Finally, the St. Venant theory [47] has been employed for the computation of the shear stress distribution over the cross-section due to torsion. Common 1D, 2D and 3D finite element solutions obtained with the commercial software MSC Nastran [48] are also included as references (rows 4 to 6). CBEAM two-node beam elements, QUAD4 four-node plate elements and HEXA8 eight-node brick elements are used respectively for the reference solutions. All the Nastran models included in this work have been built as a result of convergence analyses so as to allow fair comparison (also in terms of DOFs) with the refined beam models proposed.

Rows 7 to 12 of Table 1 show the solutions of the HLE models from the 3rd (HL3) to the 8th (HL8) expansion orders. The beam model developed for this case of study consists of 20 four-node Lagrange-type elements along the axis. The cross-section has been generated employing three Legendre-type expansion domains: one for the curved segment and one for each flange. The mapping technique here adopted allows to capture the exact geometry of the curved segment, avoiding to introduce any error due to the discretization. The FEM meshing procedure is shown in Fig. 5(a) and the cross-section domain distribution in Fig. 5(b). Unlike LE and thanks to the capabilities of HLE (see Carrera et al. [42]), the expansion order is set as an input that can be increased up to a desired accuracy without varying the longitudinal mesh or the cross-sectional domain distribution. For the sake of clarity, the displacement field of a single Legendre-type expansion domain of third order (HL3) is reported in the following
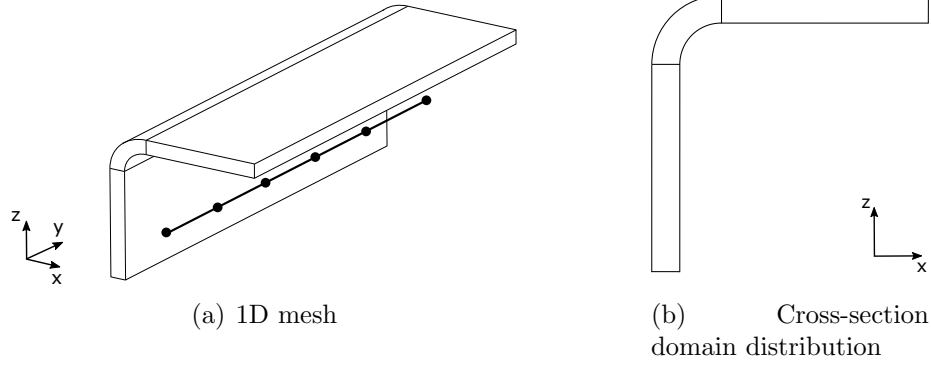
(a) 1D mesh

(b)   Cross-section domain distribution

Figure 5: L-shape beam model.

Model	$u_x \times 10^2$ m	$u_y \times 10^4$ m	$u_z \times 10^1$ m	$\sigma_{yy} \times 10^{-8}$ Pa	$\sigma_{yz} \times 10^{-6}$ Pa	$\sigma_{xy} \times 10^{-6}$ Pa	DOFs
		Point A, $y = L$		Point B, $y = 0.2$ m	Point C, $y = 0.2$ m	Point D, $y = 0.2$ m	
				Analytical solutions			
bending	9.029	-6.474	-1.388	1.869	-	-	
+ shear	9.029	-6.472	-1.389	1.869	-1.542	-0.375	
+ torsion	9.051	-6.456	-1.419	1.869	7.434	8.601	
				MSC Nastran models			
CBEAM	9.074	-6.474	-1.399	1.869	-	-	120
QUAD4	9.148	-8.684	-1.431	1.893	8.057	9.266	43750
HEXA8	9.055	-6.449	-1.419	1.874	7.546	8.701	128000
				HLE beam models			
HL3	9.000	-6.412	-1.412	1.916	7.367	8.337	5124
HL4	9.003	-6.414	-1.413	1.889	7.356	8.225	7503
HL5	9.003	-6.414	-1.413	1.892	7.408	8.475	10431
HL6	9.003	-6.414	-1.413	1.891	7.460	8.417	13908
HL7	9.003	-6.414	-1.413	1.890	7.535	8.624	17934
HL8	9.003	-6.413	-1.413	1.891	7.563	8.596	22509

Table 1: Results of displacements and stresses of the L-shape beam.

and in accordance with Eq. (1):

$$
\begin{aligned}
\mathbf{u}(x,y,z) = \ & F_1(x,z)\,\mathbf{u}_1(y) + F_2(x,z)\,\mathbf{u}_2(y) + F_3(x,z)\,\mathbf{u}_3(y) + F_4(x,z)\,\mathbf{u}_4(y) + \\
& F_5(x,z)\,\mathbf{u}_5(y) + F_6(x,z)\,\mathbf{u}_6(y) + F_7(x,z)\,\mathbf{u}_7(y) + F_8(x,z)\,\mathbf{u}_8(y) + \\
& F_9(x,z)\,\mathbf{u}_9(y) + F_{10}(x,z)\,\mathbf{u}_{10}(y) + F_{11}(x,z)\,\mathbf{u}_{11}(y) + F_{12}(x,z)\,\mathbf{u}_{12}(y).
\end{aligned}
\tag{37}
$$

When the cross-section of the model accounts for multi-domain expansions, as in the present case, the beam kinematics are obtained by imposing continuity of the generalized displacements opportunely at the common vertex and sides of the domains, see Fig. 5(b). Obviously, the number of degrees of freedom increases as the cross-section domain distribution is refined. Moreover, in this analysis case the MITC (Mixed Interpolation of Tensorial Components) approach has been used for the HLE models to compute the shear stresses. This formulation is based on the assumed interpolation of the shear components of the stress tensor and its implementation on CUF models as well as its numerical performances when applied to higher-order theories are presented in Carrera et al. [49].

In view of the results obtained for the L-angle beam, the following remarks can be made:

- The classical analytical solutions serve as a good reference for this assessment due to

the relatively high thickness of the beam walls considered. As a consequence, the beam model of Nastran perform reasonably well for the present load case. The closeness of these solutions to the solid model of Nastran support this statement.

- The results of the HLE mapped beam models are convergent both in terms of displacements and stresses already for the fourth-order model (HL4). The HLE solutions are in good agreement with the analytical results, being the accuracy of the proposed 1D model comparable to the shell and solid Nastran models. In comparison with the Nastran models, the use of the HL4 beam model implies a reduction of 82.8 % of degrees of freedom for the shell model, and up to 94.1 % for the solid one.

- The transverse shear stress values of HLE models slightly oscillate around the reference solutions as the order of expansion increases. It is well-known that the same behaviour can be observed when performing convergence analysis with classical finite element codes. The reason is that weak-form formulations are energetically coherent (and convergent from the integral standpoint), but the solution in one point can be (locally) not accurate. This aspect is further investigated in the next section, where the convergence of the present models is investigated in energy error.

4.2 Scordelis-Lo roof

The Scordelis-Lo problem, also known as barrel vault, deals with a cylindrical shell structure that is usually used in civil engineering. It is considered part of the shell obstacle course problems, defined in Belytschko et al. [50], and, for many years, it has become a standard test for the assessment of finite element formulations. The essential mechanical and geometrical characteristics of the problem have been extensively described in the literature (see Bathe and Dvorkin [51], Zienkiewi and Taylor [52] or McNeal and Harder [53]) and they can be found in Fig. 6. The test is a membrane dominated problem and it generally serves to evaluate the ability of shell elements to deal with complex membrane states of stress. In this paper, on the other hand, the Scordelis-Lo roof problem is employed to demonstrate the higher-order capabilities of the present HLE beam theories applied to curved structures. The roof structure is supported on diaphragms on both curved edges (the displacements along x and z directions are constrained) and is free on the straight ones. The shell is loaded by its own weight, modelled as a force per area unit of -90 N/m^2 in the z direction. The vertical displacement at the midpoint of the free edges (point A) is used to assess the convergence of the different formulations presented in this work.

The scope of this test is to assess the present high-order 1D formulations in capturing complex behaviours that usually require the use of 2D and 3D elements. The refined 1D elements employed make use of curved expansions to represent the exact geometry of the cross-section. Third-order polynomials have been employed to parameterize the section into the mapping functions. Figure 7 (a) shows the finite element distribution along the y-axis of the beam. Two different finite element models are tested: Lagrange-type and Legendre-type
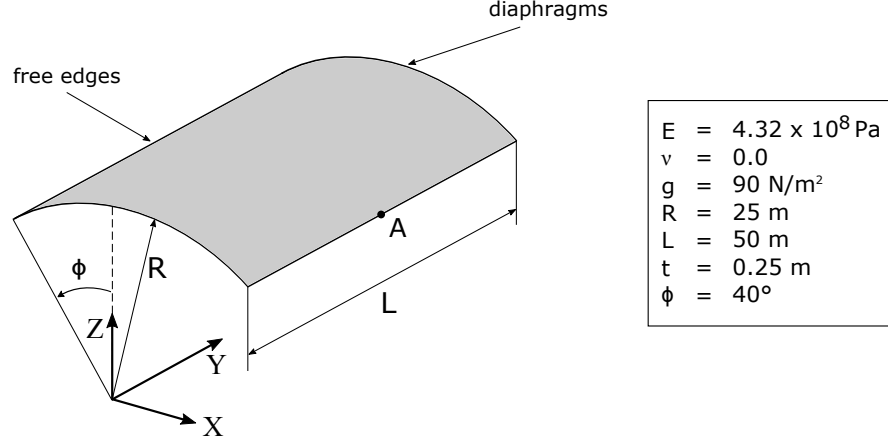
16

Figure 6: ScordelisLo roof problem geometry.
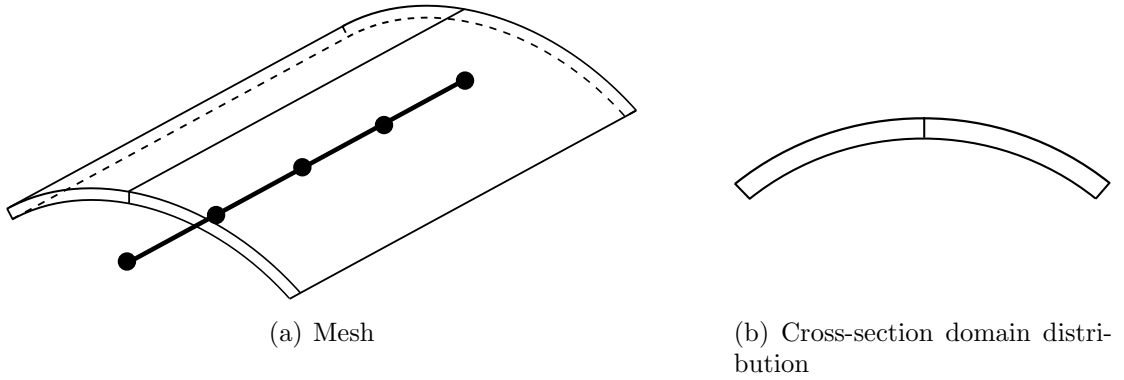

(a) Mesh

(b) Cross-section domain distribution

Figure 7: Mesh and HLE cross-section expansions used on the Scordelis-Lo roof test.

1D shape functions N_i. In the former one, the convergence of the solutions are sought by increasing both the number of elements and the polynomial order of the shape functions. On the other hand, the Legendre-type formulation has been used to develop hierarchical models. In this case, only one single element is employed along the longitudinal axis of the beam and the order is increased by following a pure p-refinement scheme. The cross-section surface has been modelled using 2 HLE curved expansion domains, as shown in Fig. 7 (b). In this paper, the penalty method is employed to apply the boundary conditions for all analysis cases.

The theoretical value for the vertical displacement quoted in the original paper of Scordelis and Lo [54] is -0.3086 m, although most finite elements models tested in the literature converge to a slightly lower value. In the present study, the solutions tend to converge to a value of -0.3079. Table 2 shows the solutions obtained by Lagrange-class HLE beam elements. Linear B2, quadratic B3 and cubic B4 finite elements are employed in configurations of 2, 4, 6 and 10 elements along the y-axis. Table 3 quotes the HLE results obtained by using Legendre-type 1D finite elements and they are referred to as P2 (quadratic) to P6 (sixth-order), depending on the polynomial space dimension. The use of Legendre-class beam elements together with HLE section expansions allows to develop fully hierarchical models for the beam analysis. Orders 2 to 8 are included for the cross-section expansions. Figures 8, 9 and 10 show the converge rates of the different models in terms of norm of the energy error

1D model	# of B2 elements				# of B3 elements				# of B4 elements			
	2	4	6	10	2	4	6	10	2	4	6	10
					Scordelis-Lo [54] u_z = -0.3086 m							
HL2	-0.0218	-0.0274	-0.0285	-0.0292	-0.0293	-0.0296	-0.0295	-0.0295	-0.0295	-0.0219	-0.0295	-0.0295
HL3	-0.2263	-0.2495	-0.2502	-0.2505	-0.2545	-0.2509	-0.2507	-0.2506	-0.2504	-0.2506	-0.2506	-0.2506
HL4	-0.2695	-0.3039	-0.3057	-0.3069	-0.3115	-0.3077	-0.3075	-0.3075	-0.3070	-0.3075	-0.3075	-0.3075
HL5	-0.2711	-0.3045	-0.3060	-0.3072	-0.3118	-0.3080	-0.3078	-0.3078	-0.3072	-0.3078	-0.3078	-0.3078
HL6	-0.2710	-0.3044	-0.3059	-0.3072	-0.3117	-0.3080	-0.3078	-0.3078	-0.3072	-0.3077	-0.3077	-0.3077
HL7	-0.2711	-0.3045	-0.3060	-0.3073	-0.3118	-0.3080	-0.3078	-0.3078	-0.3072	-0.3078	-0.3078	-0.3078
HL8	-0.2711	-0.3046	-0.3061	-0.3073	-0.3119	-0.3081	-0.3079	-0.3079	-0.3073	-0.3079	-0.3079	-0.3079

Table 2: Scordelis-Lo roof displacements at point A for Lagrange-type 1D finite elements.
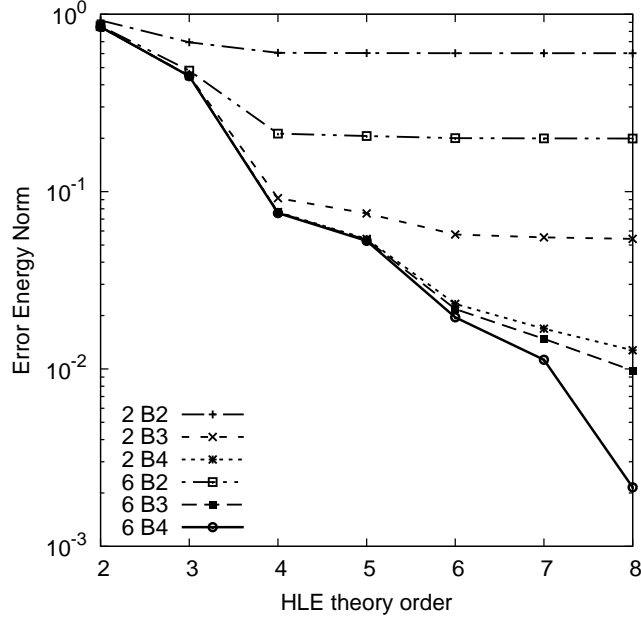

Figure 8: Convergence of the solution versus the HLE beam theory order with fixed 1D finite element mesh. Scordelis-Lo roof.

while varying the polynomial order and the number of elements. It is possible to see that convergence is reached quickly both for Lagrange and Legendre finite elements. Obviously, the higher the order of the elements, the faster the convergence is. Regarding the cross-section polynomial expansions, the study confirms that at least a four-order HL4 expansion is required to capture accurately the deformation of the section under the proposed load case. Having in mind that the parametrization of the surfaces has been conducted through cubic mapping functions, these results seem to be coherent for the authors.

The results presented in this study are compared against others from the literature in Table 4. Nastran shell and solid finite element solutions (QUAD2, QUAD4, QUAD8, HEXA8, HEX20 and HEX20R) quoted in MacNeal and Harder [53] are included, together with Koiter and Naghdi model solutions from the work of Chinosi et al. [55] and MITC hierarchical shell elements from Cinefra et al. [56]. To complete the assessment, MITC beam element solutions of HLE are also included in the table. Finally, Fig. 11 shows the deformed of the Scordelis-Lo roof from the present HL5 model with a distribution of 10 Lagrange-type beam elements.
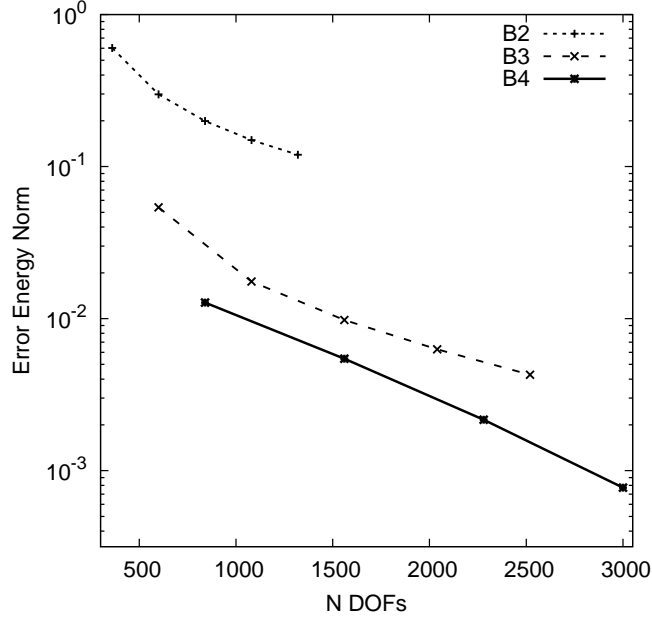
Figure 9: Convergence of the solution versus number of Lagrange-type finite elements and for a fixed theory order (HL5). Scordelis-Lo roof.

order:	P2	P3	P4	P5	P6
	Scordelis-Lo [54] u_z = -0.3086 m				
HL2	-0.0256	-0.0292	-0.0295	-0.0294	-0.0295
HL3	-0.2342	-0.2470	-0.2517	-0.2510	-0.2506
HL4	-0.2849	-0.3030	-0.3086	-0.3078	-0.3073
HL5	-0.2859	-0.3038	-0.3090	-0.3082	-0.3076
HL6	-0.2858	-0.3038	-0.3089	-0.3081	-0.3075
HL7	-0.2859	-0.3038	-0.3090	-0.3082	-0.3076
HL8	-0.2860	-0.3039	-0.3091	-0.3082	-0.3077

Table 3: Scordelis-Lo roof displacements at point A using one single Legendre-type 1D finite element.

2D and 3D elements						1D HL5 model				
Mesh	4x4	6x6	8x8	10x10	13x13	Mesh	1	2	4	10
QUAD2 [53]	0.652	0.765	0.837	0.879	-	B2	-	0.879	0.987	0.996
QUAD4 [53]	1.029	0.998	0.988	0.984	-	B3	-	1.010	0.998	0.997
QUAD8 [53]	0.964	0.982	0.977	0.976	-	B4	-	0.995	0.997	0.997
HEXA8 [53]	1.007	0.992	0.985	-	-	P3	0.984	-	-	-
HEX20 [53]	0.253	0.577	0.796	-	-	P4	1.001	-	-	-
HEX20(R) [53]	0.948	0.983	0.979	-	-	P5	0.999	-	-	-
Koiter [55]	0.957	-	-	0.977	0.980	MITC2	-	0.879	0.987	0.996
Naghdi [55]	0.957	-	-	0.978	0.982	MITC3	-	1.010	0.998	0.997
MITC LD4 [56]	0.957	-	-	0.978	0.982	MITC4	-	0.995	0.997	0.997

Table 4: Normalized vertical displacements, u/u_{ref}, found in the literature for the Scordelis-Lo roof problem against those of the HL5 beam model. u_{ref} = -0.3086 m [54].
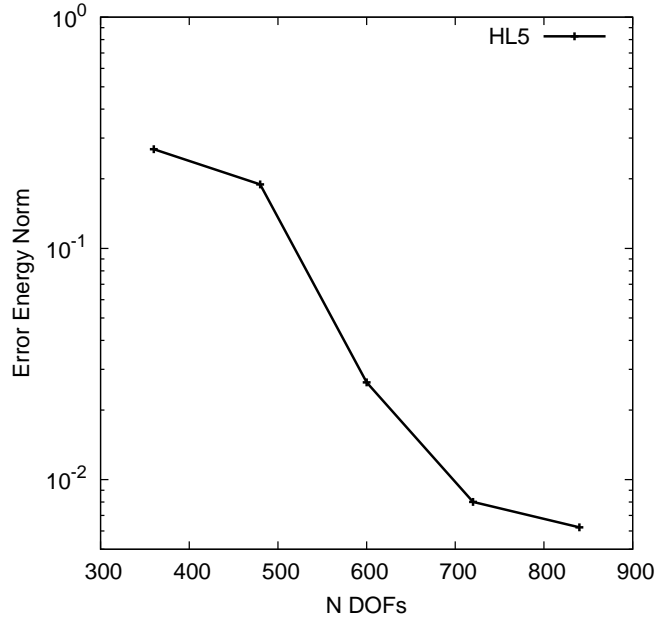
Figure 10: Convergence of the solution versus polynomial order p of one single Legendre 1D finite element with fixed theory order (HL5).
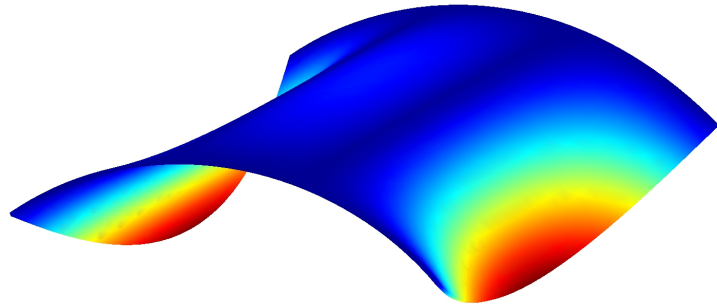

Figure 11: Scordelis-Lo roof deformed obtained through the use of 1D elements with curved high-order expansions (HL5 model).
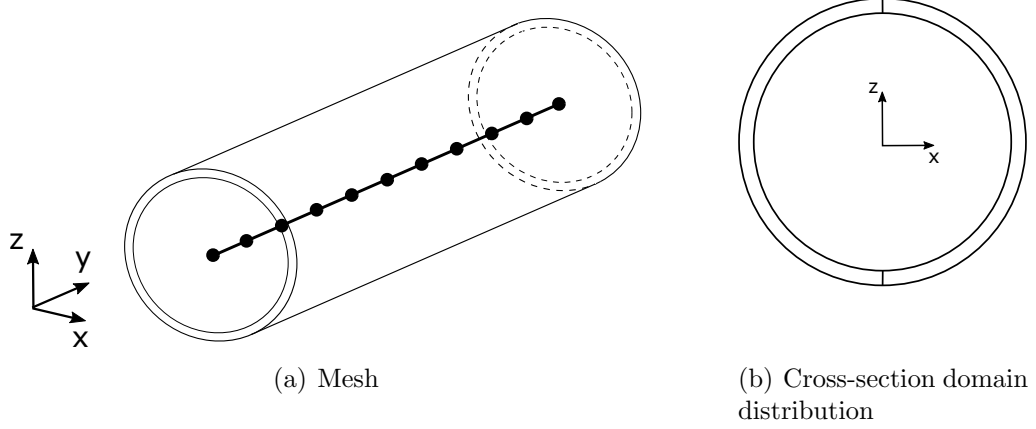
(a) Mesh   (b) Cross-section domain distribution

Figure 12: Mesh of the annular beam.

4.3   Annular cross-section beam

A clamped-clamped annular cross-section beam is now considered. This problem is similar to the well-known pinched cylinder test, also included in the aforementioned obstacle course for shell elements [50] to assess their capabilities in dealing with inextensional bending and complex states of membrane strain. Nevertheless, in order to allow for a straight comparison of the present method with other already published CUF solutions [45], the proposed analysis case differs from the original one in [50] and only one point load is applied instead of two opposite forces. The diameter of the cylinder, d, is equal to 2 m, and the thickness, t, is equal to 0.02 m. The length of the structure, L, is equal to 20 m. An isotropic material was used, with $E = 75$ GPa and $\nu = 0.33$. The cylinder is clamped at both edges and a point load F_z is applied at the top of the middle section. The force is parallel to the z-axis and its magnitude is equal to 5×10^6 N. Ten four-node Lagrange-class beam elements (B4) are used for the longitudinal mesh, as shown in Fig. 12 (a). The cross-section surface has been generated using only two expansion domains, see Fig. 12 (b). The high-order polynomials employed to map the geometry allow the section domains to adopt semi-circular shapes.

Table 5 shows the results of the vertical displacements at the loaded point. The HLE solutions are compared against others from classic, Taylor-based and shell models presented in the book of Carrera et al. [45]. TE results are included from the 1st (N=1) to the 12th order (N=12). A shell model has been created using the commercial software MSC Nastran and it is used as a reference. Both beam models converge to the shell solution with similar rates, being the computational efforts reduced in all cases. These models are capable to capture the high in-plane deformation of the mid section thanks to the use of high expansion orders. Fig. 13 shows the deformed of that section for some of the cases. It is possible to see how the deformation of the section domains becomes bigger as the expansion order of the HLE models increases.

Theory	u_z [m]	DOFs
Classical models [45]		
EBBT	-0,046	155
TBT	-0,053	155
Taylor-based models, TE [45]		
N=1	-0,053	279
N=2	-0,052	558
N=3	-0,114	930
N=4	-0,229	1395
N=5	-0,335	1953
N=6	-0,386	2604
N=7	-0,486	3348
N=8	-0,535	4185
N=9	-0,564	5115
N=10	-0,584	6138
N=11	-0,597	7254
N=12	-0,606	8463
HLE models		
HL1	-0,077	372
HL2	-0,043	930
HL3	-0,065	1488
HL4	-0,073	2232
HL5	-0,090	3162
HL6	-0,389	4278
HL7	-0,531	5580
HL8	-0,603	7068
MSC Nastran shell model [45]		
QUAD4	-0,670	49500

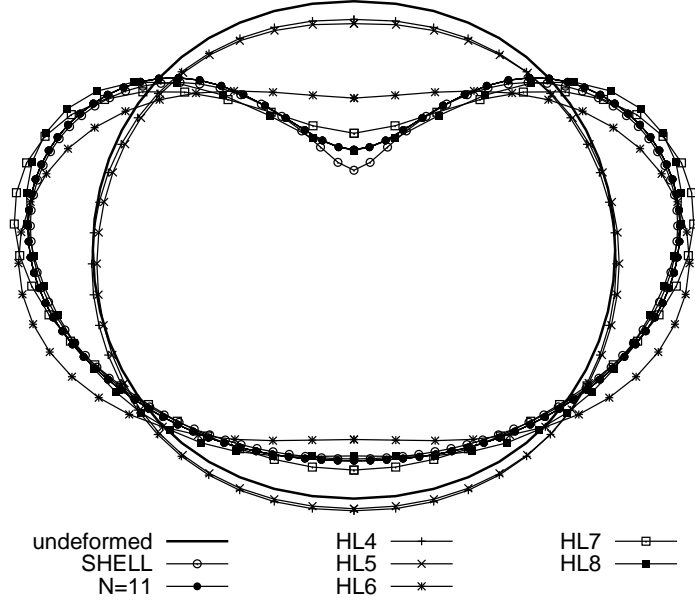Table 5: Vertical displacement, u_z, at the loaded point of the annular cross-section beam.

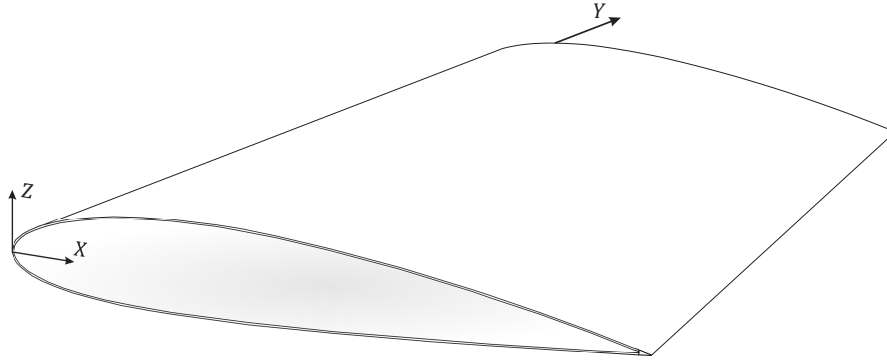Figure 13: Deformed cross-section of the annular cross-section beam.

Figure 14: Representation of the wing.

4.4 Wing structure

A benchmark wing is accounted for the last assessment. Two different configurations are considered: a monocoque wing structure and a semi-monocoque wing with spars and stringers. The airfoil chosen for this study is a NACA 2415, with a cord equal to 1 m. The thickness of the structural elements of the wing is 3 mm for the skin panels and 5 mm for the webs of both spars, when included. The wing is 6 m long and presents a clamped-free configuration. The structure is completely made of an aluminum alloy with the following characteristics: elastic modulus (E) equals to 75 GPa and Poisson ratio (ν) equals to 0.33. A single load with a magnitude of $F = -3000N$, is applied along the z-direction at 25 % of the cord at the lower surface at $y = 4$ m.

Figure 14 shows a 3D representation of the monocoque structure of the wing with respect to the global coordinate frame. The longitudinal 1D finite element mesh consist of 10 four-node Lagrange-type B4 elements. Taking advantage of the mapping techniques, the modelling of the wing section have been performed by employing only five expansion domains, as shown
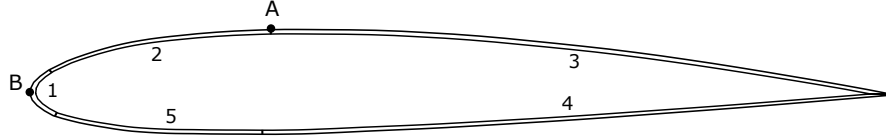
Figure 15: Cross-section domain distribution of the wing.

Model	$u_z \times 10^3$ m	$\sigma_{yy} \times 10^{-6}$ Pa	$\sigma_{yz} \times 10^{-6}$ Pa	DOFs
	Point A, $y = L$	Point A, $y = 1$ m	Point B, $y = 1$ m	
MSC Nastran solid model				
HEXA8	-85.52	38.40	-43.46	395280
Hierarchical Legendre Expansions, 10 B4				
HL2	-33.06	16.54	-60.38	2325
HL3	-83.38	37.68	-41.98	3720
HL4	-84.15	38.50	-43.81	5580
HL5	-84.76	38.55	-44.98	7905
HL6	-84.46	38.47	-44.38	10695
HL7	-84.29	38.44	-41.82	13950
HL8	-84.26	38.50	-41.81	17670
Hierarchical Legendre Expansions, 10 MITC4				
HL4	-84.15	38.50	-46.21	5580
HL8	-84.26	39.82	-44.40	17670

Table 6: Results of displacements and stresses for the monocoque wing.

in Fig. 15, with no loss of precision in the geometrical approximation.

Table 6 quotes the results of displacements and stresses. Point A is placed in the section coordinates [0.282394, 0.093267], whereas Point B corresponds to the leading edge [0, 0], see Fig. 15. A solid Nastran model has been included for comparison purposes. MITC4 beam models, developed in [49], have been also used to assess the solutions. The solutions of displacements and normal stresses show a good agreement with the ones obtained through the solid model as the polynomial order of the theory increases. Although shear stress results are quite close to the solid ones, with a maximum difference of the 3.8 % for the HL8, they can be improved by employing MITC4 beam elements instead of standard Lagrange-class ones. Finally, Fig. 16 shows the deformed of the loaded section of the wing for the solid and HL8 models.

As the final example, a complete semi-monocoque wing that includes longitudinal rein-
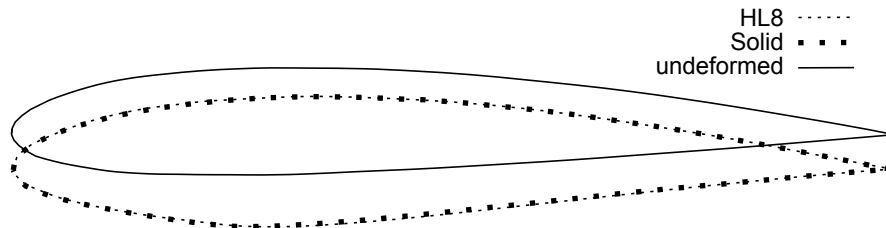

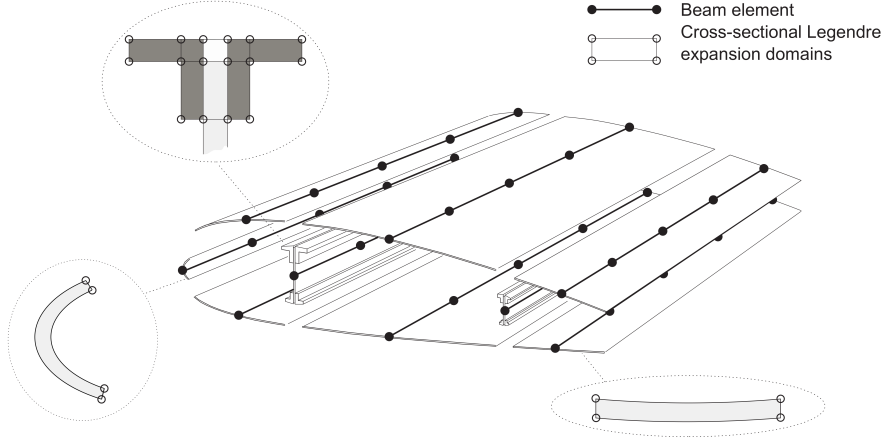Figure 16: Deformations of the loaded section of the monocoque wing.

Figure 17: Component Wise modelling using curved cross-section domains.

forcements (spars and stiffeners) is considered in the study. This kind of structures have been widely assessed in the domain of CUF by employing a Component-Wise (CW) approach, for example [39, 36, 37]. According to the CW methodology, all the components of the structure (e.g., spar, stringers, ribs, panels, etc.) are modelled by means of a CUF beam model making use of one or more expansion domains, and then assembled together at the cross-sectional level by opportunely imposing continuity of the displacements. In this way, each component of the structure is characterized by the same kinematics (i.e., same finite element) and the coupling between them is more straightforward and mathematically coherent if compared to classical FEM methods. In fact, no artificial constraints and fictitious links between the components are employed in CW methodology (see Carrera et al. [57]). Figure 17 shows the modelling procedure of HLE models through the CW approach. In this representation, it is possible to see how the use of mapping techniques on the cross-section allow to optimize the expansion domain distribution by employing large curved sub-domains, for example on the skin panels.

The displacements and stress solutions are shown in Table 7. The verification points over the cross-section are illustrated in Fig. 18, whereas their location along the axis is specified in the table. As for the previous assessment, the same load is applied at Point A. Results obtained through classic, TE and LE models in Carrera and Pagani [58] are also included for comparison purposes. Legendre-class and MITC beam element solutions are also shown for completeness. To assess these results, a solid model has been generated in the MSC Nastran software with a sufficient refined mesh that assures convergent results. Finally, the deformed of the tip section is plotted in Fig. 19 for some of these models. From these results, it is possible to state that:

- For both wing cases, HLE models show convergent solutions that are in good agreement with the solid ones used as references. Moreover, when compared against other refined beam models, CW models based on LE and HLE clearly overcome the performance of classic and TE models, which are not capable of detecting local phenomena and the stress distribution of complex structures.
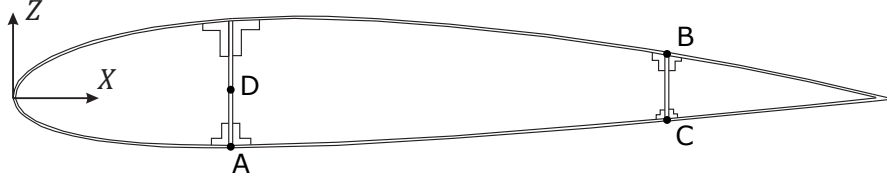
25

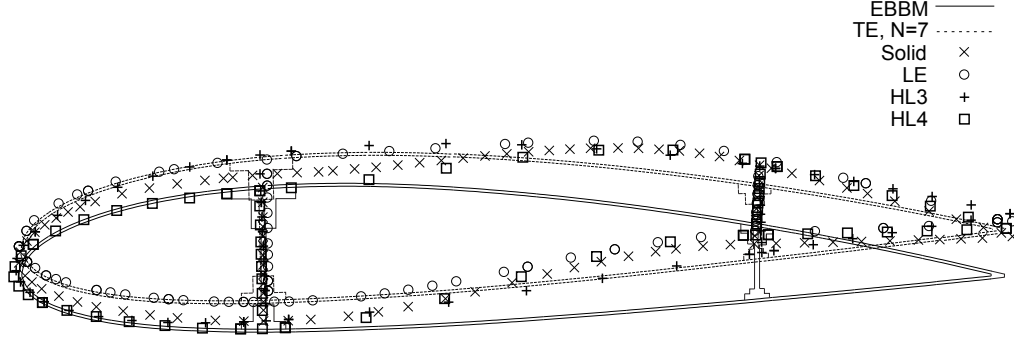Figure 18: Verification points on the wing cross-section.

Figure 19: Tip cross-section deformation of the reinforced wing.

- The higher-order expansions employed in HLE models allow them to capture complex deformation states such as bending, torsion, distorsion and in-plane warping, with the same accuracy as solid element models (see Fig. 16 and 19).

- Regarding the 1D FEM discretization, the novel hierarchical Legendre elements have demonstrated to be an interesting option when straight slender structures are considered, being capable to obtain highly accurate results with a substantial reduction of the number of degrees of freedom. Still, MITC-based beam elements are the most reliable if accurate stress distributions are desired.

5   Conclusions

This paper has discussed the use of advanced mapping techniques in the domain of higher-order one-dimensional structural theories based on the Carrera Unified Formulation (CUF). By using Legendre-like expansions of the beam kinematics, a unified finite element method has been developed straightforwardly. Arbitrary curved cross-section geometries have been taken into account accurately by employing the blending functions method.

Several structural problems aiming at verifying the enhanced characteristics of the present beam model have been addressed. These assessments include an L-shaped beam, the Scordelis-Lo roof problem, a pinched cylinder, and a wing structure for aerospace applications. The analyses have highlighted clearly three major points:

- Hierarchical Legendre Expansion (HLE) beam models based on CUF provide accurate solutions, both in terms of displacement and stress components, for all the problems

Mesh	Model	$u_z \times 10^3$ m	$\sigma_{yy} \times 10^{-6}$ Pa	$\sigma_{yz} \times 10^{-6}$ Pa	DOFs
		Point B, y = L	Point C, y = 0	Point D, y = L/2	
		MSC Nastran solid model			
HEXA8		-56.966	-19.051	-3.338	1279653
10 B4		Classic models [58]			
	EBBM	-57.519	-6.648	-	84
	TBM	-57.563	-6.647	-0.314	140
		Taylor Expansions, TE [58]			
	N=2	-55.664	-6.988	-0.339	504
	N=4	-56.401	-4.705	-2.099	1260
	N=5	-56.553	-5.308	-2.391	1764
	N=6	-56.610	-5.754	-2.470	2352
	N=7	-56.707	-6.881	-2.848	3024
	N=8	-56.731	-6.807	-2.908	3780
		CW Lagrange Expansions, LE [58]			
	LE	-56.462	-16.999	-3.182	22200
		CW Hierarchical Legendre Expansions, HLE			
	HL3	-56.776	-22.133	-2.763	37944
	HL4	-56.579	-21.651	-3.141	58218
	HL5	-56.420	-20.476	-3.319	84165
	HL6	-56.427	-20.410	-3.341	115785
10 MITC4	HL3	-56.777	-22.133	-2.765	37944
	HL4	-56.578	-21.648	-3.143	58218
	HL5	-56.419	-20.474	-3.303	84165
	HL6	-56.427	-20.410	-3.325	115785
1 P5	HL4	-55.105	-19.766	-3.175	11268
	HL5	-54.925	-19.280	-3.314	16290
	HL6	-54.929	-19.257	-3.333	22410
1 P8	HL4	-56.229	-20.182	-2.442	16902
	HL5	-56.069	-19.292	-2.600	24435
	HL6	-56.075	-19.215	-2.625	33615

Table 7: Results of displacements and stresses of the reinforced wing.

considered. HLE elements represent an excellent alternative to the state-of-the-art 2D and 3D finite elements, because of their efficiency and physical consistency.

- Blending functions method is effective when employed on the cross-section domain for the description of curved and distorted boundaries. Thanks to this method, geometric accurate and refined beam models can be implemented with relative ease.

- In the provided methodology, the description of the cross-section domain is fixed and the accuracy is controlled by the polynomial order of the theory. As a consequence, there is no need to perform iterative refinements for increasing the kinematics and the geometrical accuracy with a considerable saving of modelling times.

The proposed mapping technique enables the efficient analysis of a broad class of structures regardless of the geometrical complexity of the cross-section. In addition, the non-local expansion capabilities of the beam model make it possible to obtain the complete state of stress of the structure of thin-walled beams and shell-like structures for different kinds of boundary conditions. The results of this research provide good confidence for future extension to global/local and multi-scale analysis of composite structures.

Acknowledgements

References

[1] L. Euler. *De curvis elasticis.* Lausanne and Geneva: Bousquet, 1744.

[2] S. P. Timoshenko. On the transverse vibrations of bars of uniform cross section. *Philosophical Magazine*, 43:125–131, 1922.

[3] R.K. Kapania and S. Raciti. Recent advances in analysis of laminated beams and plates, part I: Shear effects and buckling. *AIAA Journal*, 27(7):923–935, 1989.

[4] R.K. Kapania and S. Raciti. Recent advances in analysis of laminated beams and plates, part II: Vibrations and wave propagation. *AIAA Journal*, 27(7):935–946, 1989.

[5] E. Carrera, A. Pagani, M. Petrolo, and E. Zappino. Recent developments on refined theories for beams with applications. *Mechanical Engineering Reviews*, 2(2):1–30, 2015.

[6] J. N. Reddy. On locking-free shear deformable beam finite elements. *Computer Methods in Applied Mechanics and Engineering*, 149:113–132, 1997.

[7] R. U. Vinayak, G. Prathap, and B. P. Naganarayana. Beam elements based on a higher order theory - I. Formulation and analysis of performance. *Computers & Structures*, 58(4):775–789, 1996.

[8] F. Gruttmann, R. Sauer, and W. Wagner. Shear stresses in prismatic beams with arbitrary cross-sections. *International Journal for Numerical Methods in Engineering*, 45:865–889, 1999.

[9] W. Wagner and F. Gruttmann. A displacement method for the analysis of flexural shear stresses in thin-walled isotropic composite beams. *Computers & Structures*, 80:1843–1851, 2002.

[10] J. Petrolito. Siffness analysis of beams using a higher-order theory. *Computers & Structures*, 55(1):33–39, 1995.

[11] R. Schardt. Verallgemeinerte technische biegetheorie. *Springer-Verlag*, 1989. in German.

[12] J.M. Davies and P. Leach. First-order generalised beam theory. *Journal of Constructional Steel Research*, 31(2):187 – 220, 1994.

[13] J.M. Davies, P. Leach, and D. Heinz. Second-order generalised beam theory. *Journal of Constructional Steel Research*, 31(2):221 – 241, 1994.

[14] N. Silvestre and D. Camotim. First-order generalised beam theory for arbitrary orthotropic materials. *Thin-Walled Structures*, 40(9):755 – 789, 2002.

[15] N. Silvestre and D. Camotim. Second-order generalised beam theory for arbitrary orthotropic materials. *Thin-Walled Structures*, 40(9):791 – 820, 2002.

[16] N. Silvestre. Generalised beam theory to analyse the buckling behaviour of circular cylindrical shells and tubes. *Thin-Walled Structures*, 45:185–198, 2007.

[17] J.C. Simo and L. Vu-Quoc. A Geometrically-exact rod model incorporating shear and torsion-warping deformation. *International Journal of Solids and Structures*, 27(3):371 – 393, 1991.

[18] P.M. Pimienta and E.M.B. Campello. A fully nonlinear multi-parameter rod model incorporating general cross-section in-plane changes and out-of-plane warping. *Latin American Journal of Solids and Structures*, 1(1):119 – 140, 2003.

[19] R. Gonçalves, M. Ritto-Corra, and D. Camotim. A large displacement and finite rotation thin-walled beam formulation including cross-section deformation. *Computer Methods in Applied Mechanics and Engineering*, 199(2324):1627 – 1643, 2010.

[20] E.M.B. Campello and L.B. Lago. Effect of higher order constitutive terms on the elastic buckling of thin-walled rods. *Thin-Walled Structures*, 77:8 – 16, 2014.

[21] E. Carrera. Theories and finite elements for multilayered, anisotropic, composite plates and shells. *Archives of Computational Methods in Engineering*, 9(2):87–140, 2002.

[22] E. Carrera. Theories and finite elements for multilayered plates and shells: a unified compact formulation with numerical assessment and benchmarking. *Archives of Computational Methods in Engineering*, 10(3):216–296, 2003.

[23] E. Carrera and G. Giunta. Refined beam theories based on Carrera's unified formulation. *International Journal of Applied Mechanics*, 2(1):117–143, 2010.

[24] B. Szabó and I. Babuka. *Finite Element Analysis.* John Wiley and Sons, Ltd, 1991.

[25] W.J. Gordon and C.A. Hall. Transfinite element methods: Blending-function interpolation over arbitrary curved element domains. *Numerische Mathematik*, 21(2):109–129, 1973.

[26] A. Düster, H. Bröker, and E. Rank. The p-version of the finite element method for three-dimensional curved thin walled structures. *International Journal for Numerical Methods in Engineering*, 52(7):673–703, 2001.

[27] G. Királyfalvi and B. Szabó. Quasi-regional mapping for the p-version of the finite element method. *Finite Elements in Analysis and Design*, 27(1):85 – 97, 1997. Robert J. Melosh Medal Competition.

[28] T.J.R. Hughes, J.A. Cottrell, and Y. Bazilevs. Isogeometric analysis: CAD, finite elements, NURBS, exact geometry and mesh refinement. *Computer Methods in Applied Mechanics and Engineering*, 194(3941):4135 – 4195, 2005.

[29] K. Washizu. *Variational Methods in Elasticity and Plasticity.* Pergamon, Oxford, 1968.

[30] M. Petrolo E. Carrera, G. Giunta. *Beam structures: classical and advanced theories.* John Wiley and Sons, 2011.

[31] E. Carrera, M. Petrolo, and E. Zappino. Performance of CUF approach to analyze the structural behavior of slender bodies. *Journal of Structural Engineering*, 138(2):285–297, 2012.

[32] E. Carrera, A. Pagani, and M. Petrolo. Use of Lagrange multipliers to combine 1D variable kinematic finite elements. *Computers & Structures*, 129:194–206, 2013.

[33] E. Carrera and A. Pagani. Analysis of reinforced and thin-walled structures by multi-line refined 1D/beam models. *International Journal of Mechanical Sciences*, 75:278–287, 2013.

[34] E. Carrera and A. Pagani. Evaluation of the accuracy of classical beam FE models via locking-free hierarchically refined elements. *International Journal of Mechanical Sciences*, 100:169–179, 2015.

[35] E. Carrera and M. Petrolo. Refined beam elements with only displacement variables and plate/shell capabilities. *Meccanica*, 47(3):537–556, 2012.

[36] E. Carrera, M. Maiarù, and M. Petrolo. Component-wise analysis of laminated anisotropic composites. *International Journal of Solids and Structures*, 49:1839–1851, 2012.

[37] E. Carrera, A. Pagani, and M. Petrolo. Component-wise method applied to vibration of wing structures. *Journal of Applied Mechanics*, 80(4):041012, 2013.

[38] E. Carrera, A. Pagani, and M. Petrolo. Classical, refined and component-wise theories for static analysis of reinforced-shell wing structures. *AIAA Journal*, 51(5):1255–1268, 2013.

[39] E. Carrera, A. Pagani, and M. Petrolo. Refined 1D finite elements for the analysis of secondary, primary, and complete civil engineering structures. *Journal of Structural Engineering*, 141(4):art. no. 04014123, 2014.

[40] E. Carrera and A. Pagani. Free vibration analysis of civil engineering structures by component-wise models. *Journal of Sound and Vibration*, 333(19):4597–4620, 2014.

[41] E. Carrera, A. Pagani, and R. Jamshed. Refined beam finite elements for static and dynamic analysis of hull structures. *Comput. Struct.*, 167(C):37–49, April 2016.

[42] E. Carrera, A.G. de Miguel, and A. Pagani. Hierarchical theories of structures based on legendre polynomial expansions with finite element applications. *International Journal of Mechanical Sciences*, 2016. In Press. DOI: 10.1016/j.ijmecsci.2016.10.009.

[43] B. Szabó, A. Dster, and E. Rank. *The p-Version of the Finite Element Method*. John Wiley and Sons, Ltd, 2004.

[44] A. Pagani, A.G. de Miguel, M. Petrolo, and E. Carrera. Analysis of laminated beams via unified formulation and Legendre polynomial expansions. *Composite Structures*, 156:78–92, 2016.

[45] E. Carrera, M. Cinefra, E. Zappino, and M. Petrolo. *Finite Element Analysis of Structures Through Unified Formulation*. John Wiley and Sons, Ltd, 2014.

[46] V.Z. Vlasov. *Thin-walled elastic beams*. Israel Program for Scientific Translations, 1961.

[47] B. SaintVenant. Memoire sur la torsion des prismes. *Mem. Acad. Sci. Savants Etrangers*, 14:233–560, 1855.

[48] MSC.Software Corporation. MD Nastran 2010 Quick Reference Guide. 2010.

[49] E. Carrera, A.G. de Miguel, and A. Pagani. Extension of MITC to higher-order beam models and shear locking analysis of compact, thin-walled and composite structures. 2016. Submitted.

[50] T. Belytschko, H. Stolarski, W.K. Liu, N. Carpenter, and Ong J.S.-J. Stress projection for membrane and shear locking in shell finite elements. *Comput. Methods Appl. Mech. Engrg*, 51:221258, 1985.

[51] K-J. Bathe and E. N. Dvorkin. A formulation of general shell elementsthe use of mixed interpolation of tensorial components. *International Journal for Numerical Methods in Engineering*, 22(3):697–722, 1986.

[52] O.C. Zienkiewicz and R.L. Taylor. *The finite element method*, volume 3. McGraw-hill London, 1977.

[53] R.H. Macneal and R.L. Harder. A proposed standard set of problems to test finite element accuracy. *Finite Elements in Analysis and Design*, 1(1):3 – 20, 1985.

[54] A.C. Scordelis and K.S. Lo. Computer analysis of cylindrical shells. *J. Am. Concrete Inst.*, 61:561593, 1964.

[55] C. Chinosi, L. Della Croce, and T. Scapolla. Hierarchic finite elements for thin Naghdi shell model. *International Journal of Solids and Structures*, 35(16):1863 – 1880, 1998.

[56] M. Cinefra, C. Chinosi, and L. Della Croce. MITC9 shell elements based on refined theories for the analysis of isotropic cylindrical structures. *Mechanics of Advanced Materials and Structures*, 20(2):91–100, 2013.

[57] E. Carrera, A. Pagani, and M. Petrolo. Classical, refined, and component-wise analysis of reinforced-shell wing structurescomponent-wise method applied to vibration of wing structures. *AIAA Journal*, 51(5):1255–1268, 2013.

[58] E. Carrera and A. Pagani. Accurate response of wing structures to free-vibration, load factors, and nonstructural masses. *AIAA Journal*, 54(1):227–241, 2016.